RSC Advances

ROYAL SOCIETY OF CHEMISTRY

www.rsc.org/advances

TOC/Abstract art of present work

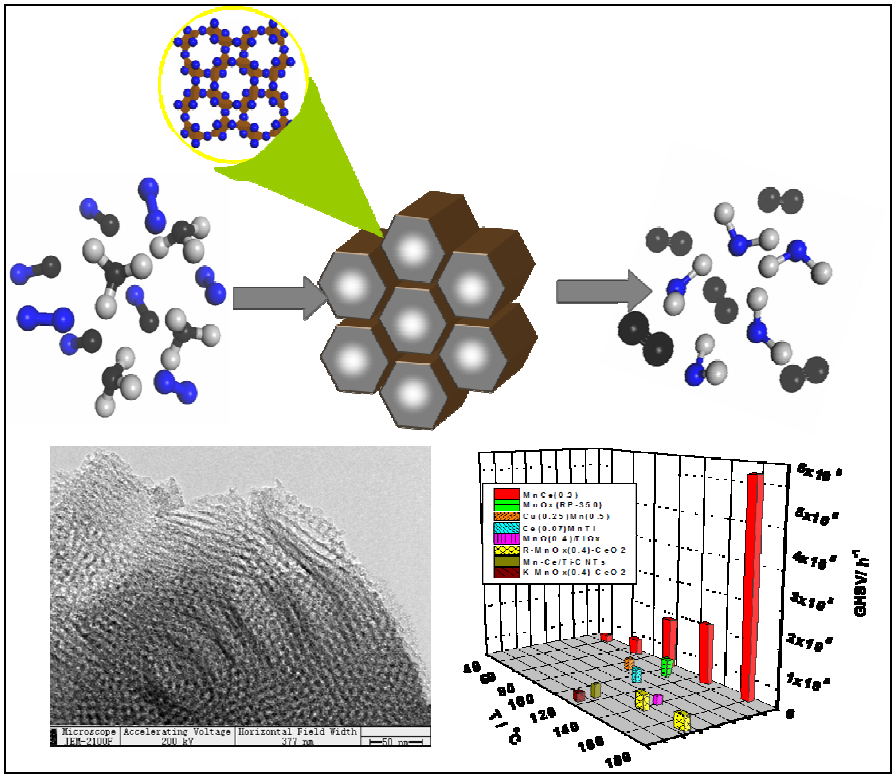

Due to high surface area and 3-D meso-channel, the catalyst exhibit high performance on NH_3-SCR for NO

Cite this: DOI: 10.1039/c0xx00000x

www.rsc.org/xxxxxx

communication

MnO_2 doped CeO_2 with tailored 3-D channel exhibit excellent performance for NH_3-SCR of NO

Yajuan Wei[a], Yan Sun[a], Wei Su[b], Jia Liu*[b]

Received (in XXX, XXX) Xth XXXXXXXXX 20XX, Accepted Xth XXXXXXXXX 20XX

DOI: 10.1039/b000000x

Diffusion behaviours during the NO conversion by NH_3-SCR were simulated by molecular dynamic method. $MnCeO_x$ with tailor 3-D channel was obtained from templates KIT-6. The remarkable performance on NH_3-SCR results from a large surface area for chemisorption and an appropriately sized channel for mass diffusion.

Introduction

NO_x are unavoidable during the combustion of fossil fuels. Unfortunately, the world will continue to rely on the fossil fuel as the primary energy for a long term. As is well known, selective catalytic reduction (SCR) is one of the most effective methods for NO removal that has been practical proven.[1] Commercial catalysts such as V_2O_5/TiO_2 and V_2O_5-WO_3/TiO_2 have been frequently employed due to their high activity for NO_x removal.[2, 3] However they also suffer from contaminations from SO_2 and fly ash. A simple solution is placing SCR system following the de-sulfurizer with a temperature range of 80 °C-175 °C. So steps of improving low temperature activity for SCR never stop. Manganese based catalysts exhibit high activities at low temperature which have been well proven.[4-32] NO conversion over $Mn_xCo_{3-x}O_4$ nano-cages with surface area of 77 $m^2.g^{-1}$ was about 90 % at 125 °C while that was about 40 % over nano-partical $Mn_xCo_{3-x}O_4$ with areas of 33 $m^2.g^{-1}$ at the same condition which reported by Lei Zhang.[24] The highest activity for SCR were present on Ni(0.4)-MnO_x (400 °C) which owned the largest surface area (90.5 $m^2.g^{-1}$) in their series catalysts prepared by Yaping Wan.[25] It is evident that surface area plays an important role in SCR. MnO_x supported on porous materials (nano-tube, activated carbon, molecular sieves and silicon materials etc) in order to enhance the surface areas has been well studied[5, 6, 26]. Mn–Ni(0.4)/TiO_2 catalyst reported by Panagiotis G. Smirniotis showed a remarkable performance by exhibiting 100% NO conversion at 200 °C with a GHSV of 50000 h^{-1} [27]. Mn/FER, Mn/Mont-10, Mn/ETS-10 and Mn/TiO_2 were prepared by Asima Sultana[28] on which NO conversions were about 90 % at a temperature range from 160 °C to 400 °C. MnCe@CNTs-R and Mn(25 %)Ce(28 %)/CNTs-S prepared by Dengsong Zhang[9, 29] exhibited the best activities at about 220 °C which NO conversion levels up to 95 %. Tae Sung Park[30] investigated activity of MnO_2/γ-Al_2O_3 with surface area of 243 $m^2.g^{-1}$ for NH_3-SCR on which NO conversion leveled up to 100% cross the temperature range of 150 °C to 250 °C.

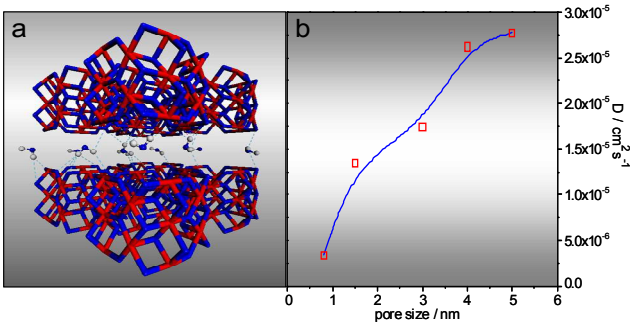

Figure 1. (a) water diffusion in a slit pore; (b) water diffusion coefficients in different sized pore

Another factor the same important as surface area is pore size. The pore size of MnO_2 doped Fe_2O_3 hollow nano-fibers have been successfully enlarge to 6-8 nm by using electrospinning method which exhibited nearly 100 % of NO conversion from 150 °C to 300 °C.[31] By using Pluronic F127 as pore agent, a series of hierarchically Mn/TiO_2 catalysts have been synthesized by Yanni Shi, among which HM(0.012)-Mn/TiO_2 with the surface area of 112 $m^2.g^{-1}$ and macro-meso pore exhibited the NO conversion of 100 % at 100 °C.[32] It is obvious that the pore size has great influence on SCR reaction. However to the best of our knowledge, the mechanism is still unclear.

Molecular dynamic Simulation

During the SCR process NO are converted to N_2 as the following equation:

$$4NH_3 + 4NO + O_2 \rightarrow 4N_2 + 6H_2O \quad (1)$$

Comparing with reactants and other products, produced water diffuse difficultly especially in micro-pore shown as Figure. 1 (a) which result from strong hydrogen bonds combined with the superficial oxygen on the catalysts.

Increasing pore size appropriately can ameliorate diffusion. However large pore size generally results in a low space efficiency which is not what we want. So water diffusion behaviours in slits with different size were simulated. Diffusion coefficients were calculated from mean square displacement (MSD) curves shown in Figure S1 (Supporting information) according to Einstein equation. The details were descripted in Supporting Information and the results were list in Table S1. It is found that the diffusion coefficient increase with a increasing of slit size then slowly when the slit size is larger than 4 nm (Figure

1. b). In the slit > 4 nm the hydrogen bonds mainly come from the single surface of MnO_2. Adsorptive interaction from the opposite is insufficient. Probability of collision with the opposite side is considerable low. Diffusion in the slit larger than 4 nm is similar as it on an open surface. As a result, slit size of 4 nm is enough for water diffusion during the SCR reaction.

Experiments

According to the simulation results, Mn based catalyst with high surface area and tailored three dimensional channels was prepared by using KIT-6 as templates and applied in denitrification for the first time. N_2 isotherm at 77 K was collected for surface area and pore size calculation. Powder X-Ray Diffraction (PXRD), Transmission Electron Microscopy (TEM), Energy Dispersive Spectrometer (EDS) and X-ray Photoelectron Spectroscopy (XPS) were performed for structure and component analysis. The low temperature activities for SCR of NO were tested. Effects of temperature and gas hourly space velocities (GHSV) were present.

All reagents were analytical grade purchased from Alfa Aesar and deionized water was used for catalysts synthesis. KIT-6 were prepared as the templates with BET surface areas of 888 $m^2.g^{-1}$ according the reference[33].77 K N_2 isotherm on KIT-6 were present in Figure S2 (Supporting Information) and pore distribution calculated by BJH method were shown in Figure S3 (Supporting Information).

Catalysts ($MnCeO_x$) were synthesized by dissolving the corresponding amounts of $Ce(NO_3).6H_2O$ (0.002mol) and $Mn(AC)_2.4H_2O$ (0.006 mol) in 30 ml of deionized water, followed by adding 2 g of KIT-6 as the templates. The resulting slurry was stirring at 80 ^oC until dry. The pale pink powders were finally calcined at 400 ^oC for 4 hours in air ambient. After cooling into room temperature the dark brown powder was soaked in 100 ml NaOH solution (4 $mol{\cdot}L^{-1}$) with constantly stirring for 20 min at 70 ^oC for template removal. Subsequently filter and wash with deionized water until PH value reached 7. The obtained solids were dried overnight at 120 ^oC in vacuum and crushed to 60-80 mesh for experiments.

The equipment used to measure the catalytic activities is shown in Scheme S2 (Supporting Information). The mixture gas continuous flow stainless steel reactor (i.d=4mm) with volume of 0.47 ml, 300 mg catalyst (60–80 mesh) was compacted in the reactor for each test. The NO, NO_x and NH_3 concentration of inlet and outlet gases were measured by an FTIR spectrometer Model QGS-08C purchased from Beijing BAIF-Maihak Analytical Instrument Co. Ltd. All the feed gas purchased by Beijing AP BAIF Gas Industry Co. Ltd. (Beijing, China) (1000 ppm NO, 1000ppm NH_3, 21% O_2 all balanced by N_2). Each flow rate was controlled by mass flow controllers, Model SY9312 purchased from Beijing Shengye Sci. & Tech. Dev. Co. The mixed gas for test consisted of NO (0.04%), NH_3 (0.04%), O_2 (4%) balanced by N_2.

Results and Discussion

N_2 Isotherm at 77 was collected by Surface Area Analyzer Micromeritics (ASAP 2020) which was shown in figure 2 (a). Surface areas of 340 $m^2.g^{-1}$ and pore volume of 0.45 $cm^3.g^{-1}$ were

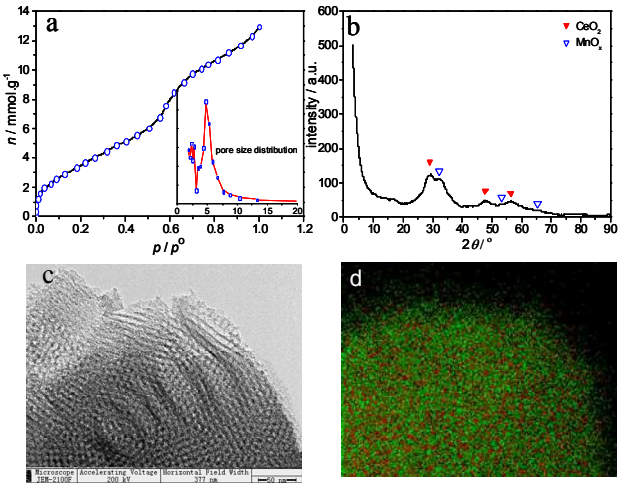

Figure 2. (a) N_2 isotherm of catalyst at 77 K (b) PXRD pattern of catalyst; (c) Tem image of catalysts; (d) EDX mapping of catalysts.

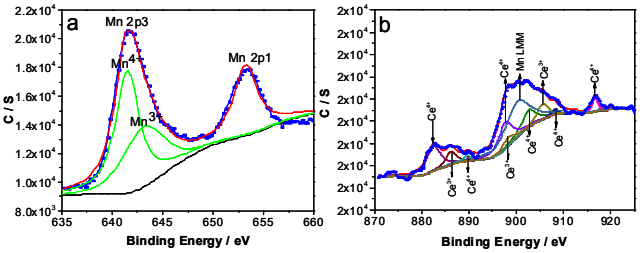

Figure 3. Mn Ce XPS spectra of meso-porous catalysts

calculated by BET method and N_2 uptakes at p/p^o (0.995) respectively. The pore size focused on 4.8 nm calculated from BJH method.

Diffraction (PXRD) patterns were recorded on a Rigaku D/max 2250VB/PC diffract meter (Rigaku, Japan) with CuKα radiation (λ = 1.5406 A °). Diffraction peaks of MnO_x and CeO_2 were observed in figure 2(b). The wide half peak width illustrate that the structure of catalyst are almost amorphous. Three dimensional porous structures were proven by TEM image (figure 1, c). Mn and Ce were dispersing well in the catalyst which has been proven by EDX mapping image (Figure 2 d).

XPS analysis were perform on ESCALAB 250 multi-technique X-ray photoelectron spectrometer (UK) using a monochromatic AlKα X -ray source (hv=1486.6 eV). All XPS spectra (Figure S4, supporting information) were recorded using an aperture slot of 300×700 microns, and survey spectra were recorded with pass energy of 160 eV, and high resolution spectra with pass energy of 29.35 eV. 20 scans per region were taking with a step size of 0.25eV. Two main peaks shown in Figure 3(a) can be observed from 642 eV to 660 eV due to Mn 2p3/2 and Mn 2p1/2. By performing a peak-fitting deconvolution, the Mn 2p3/2 spectra were separated into two peaks, Mn3+ (640 eV) and Mn4+ (641.6 eV). It also was observed from XRD results. As shown in Fig.3 b, the complicated satellite structures were observed in Ce3d XPS spectrum. The Ce3d XPS peaks are labelled for identification. The results indicate the cerium in the catalyst present in both Ce^{4+} and Ce^{3+} oxidation states.[34, 35] The ratio of Ce/Mn on the surface was approximate 0.26. It is noteworthy that O content on the surf-

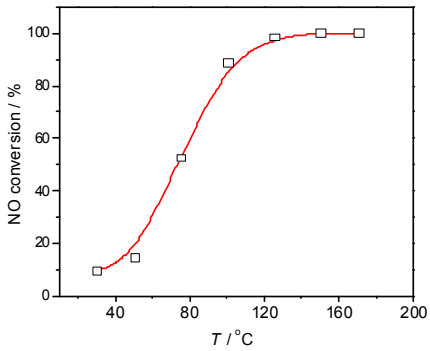

Figure 4. Effect of temperature on NO conversion with GHSV 8.9×10^4 h^{-1}

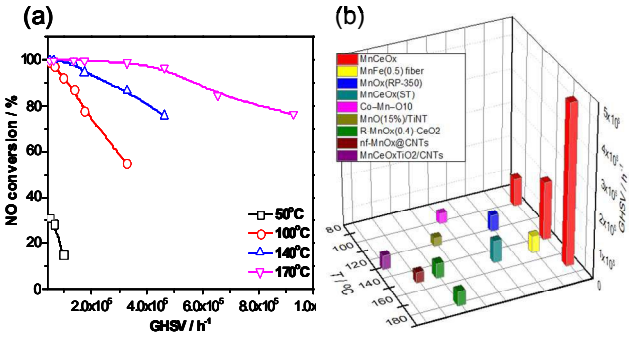

Figure 5. (a) Effect of GHSV on NO conversation; (b) comparison of GHSV with other catalyst.[9, 10, 31, 36-40]

ace is about 36.4% (Supporting Information) that is more than the theoretical O content in the lattice of $MnCeO_x$. The over content of oxygen may be attributed to chemisorbed oxygen on the surface which is beneficial to oxidation process during the NH_3-SCR.[41, 42]

Catalyst performances were tested at a temperature range as low as 50 °C to 175 °C. Present in Figure 4 the NO conversion yield 60% at 75 °C. With a raising of temperature from 30 °C to 100 °C NO conversion level up from 17.4 % to 100 %. NO conversion kept at a high value of 100 % when the temperature was greater than 100 °C with a GHSV of 89000 h^{-1}. Below 80 °C the produced water diffuses difficultly and occupies the active sites on $MnCeO_x$ thereby restricting the reaction processing. Above 100 °C the metallic surface can be refreshed in time because that the adsorptive water molecules overcome the constraint and disperse from the pore. On the other hand, the molecules were supplied enough energy for overcoming the active energy barrier with a increasing of temperature. From views of reaction kinetic and diffusion, high temperature is benefit to NO conversion.

GHSV is an important criterion to estimate catalytic activity. Under a relative low GHSV, the molecules contact the surface intensively result in a complete conversion. With increasing of GHSV NO conversion degrade (Figure 5, a) which results from restriction of diffusion rate and chemical reaction rate. Increasing temperature the molecules were supplied enough energy result in an enhancing of collision frequency and to overcome the active energy barrier. Gas molecules can be adsorbed on active sites and dispersed from inner pores immediately at high temperature even under a high GHSV.

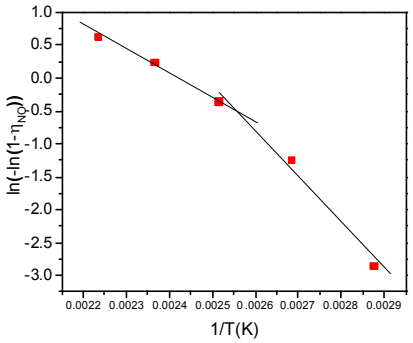

Figure 6. Arrhenius plots of NO conversion

Targeting NO conversion at 95 % the maxim value of GHSV has been present in figure 5(b) and compared with reported results. It is evident that the GHSV in present work is much higher than others in the same conditions due to the high surface area (340 $m^2.g^{-1}$) and probably channel size (4.8nm). The maxim value of GHSV was respectively 480000 h^{-1} at 170 °C and 89000 h^{-1} at 100°C.

Insight into kinetics was studied. The NH_3-SCR on the MnO_x–CeO_2 was generally considered being a first-order reaction with respect to NO.[12] The effective first-order rate constant is related to NO conversion (η NO) by following equation:

$$k = -\frac{F}{A_R}\ln\left(\frac{C_{no,out}}{C_{no,in}}\right) = -\frac{F}{A_R}\ln(1-\eta_{NO}) = -A_f\ln(1-\eta_{NO}) \quad (2)$$

Where k is first-order rate constant ($cm^3.g^{-1}.min^{-1}$) of reaction, F is gas flow rate ($cm^3.min^{-1}$), A_f is catalysts surface area ($cm^2.g^{-1}$)

According to Arrhenius formula there is the following relation

$$k = P\exp(-\frac{Ea}{RT}) \quad (3)$$

$$\ln(-\ln(1-\eta_{NO})) = \ln(P / A_f) - Ea / RT \quad (4)$$

Ea is the apparent activation energy ($kJ.mol^{-1}$), R is the gas constant (8.314 $J.mol^{-1}.K^{-1}$), and T is the temperature (K), P is pre-exponential factor. Apparent activation energy and pre-exponential factor can be calculated from the slope and intercept of the plots of ln(-ln(1- η)) to 1/T. NO conversions of $MnCeO_x$ (300 mg) were determined with GHSV of 656500 h^{-1} cross a temperature range of 75 °C to 175 °C for Ea calculation. The results were listed in Table S2 (Supporting Information).

The plots of ln(-ln(1-η_{NO})) vs 1/T were shown in Figure 6. According to the difference of the slope the plots could be divided into low temperature section (75 °C- 125 °C) and high temperature section (125 °C -175 °C). Apparent activation energy and pre-exponential factor of each section were yield summed in Table S3 (supporting information).

The low Ea value and low per-exponential factor demonstrate that the SCR reaction rate is controlled by diffusion at high temperature. Gas molecular must diffuse into the meso-pore first then adsorbed on the surface of catalysts before conversions happen. The produced water can not depart from the surface immediately and occupy active sites lead to reaction rate

reducing. While high temperature is beneficial to diffusion and enhancing collision frequency. Both of them can improve the reaction rate and NO conversion. Per-exponential factor increased sharply with temperature increasing which supported the above conclusions.

Conclusions

In summary, water diffusion behaviours on MnO_2 were simulated by molecular dynamic method. The optimal slit size of 4 nm was obtained by analysis. By using a template method $MnCeO_x$ with tailored 3-D channels was successful synthesized. A flying improvement of low-temperature NH_3-SCR activity was shown on $MnCeO_x$ with surface area of 340 $m^2.g^{-1}$ and 3-D porous structure. NO conversion can reach above 95 % at a temperature as low as 100 ^oC with GHSV of 89000 h^{-1} or at a temperature of 170 ^oC with high GHSV of 480000 h^{-1}. Kinetic analysis demonstrated that SCR reaction was controlled by diffusion above 125 ^oC. Catalyst designed for NO conversion in the letter is quite promising in overcoming the current bottleneck of SCR technology.

Acknowledgments

This work was supported by National Natural Science Foundation of china (21206108), National Natural Science Foundation of china (21406004) and Tian Jin Natural Science Foundation (10JCZDJC23900)

Notes and references

[a] *Department of Chemistry, School of Science Tianjin University, Tianjin 300072, PR China*
[b] *High Pressure Adsorption Laboratory, School of Chemical Engineering & Technology Tianjin University, Tianjin 300072, PR China,*
E-mail: liujia@ntu.edu.sg

1. S. i. Matsumoto, Y. Ikeda, H. Suzuki, M. Ogai and N. Miyoshi, *Applied Catalysis B: Environmental*, 2000, **25**, 115.
2. G. Liu and P.-X. Gao, *Catalysis Science & Technology*, 2011, **1**, 552.
3. H. Chang, M. T. Jong, C. Wang, R. Qu, Y. Du, J. Li and J. Hao, *Environmental Science & Technology*, 2013, **47**, 11692.
4. B. Thirupathi, P.G. Smirniotis, *Applied Catalysis B: Environmental*, 2011, **110**,195.
5. J. Yu, F. Guo, Y. Wang, J. Zhu, Y. Liu, F. Su, S. Gao, G. Xu, *Applied Catalysis B: Environmental*, 2010, **95**, 160.
6. P.G. Smirniotis, D.A. Peña, B.S. Uphade, *Angewandte Chemie International Edition*, 2001, **40**, 2479-2482.
7. M. Casapu, O. Kröcher and M. Elsener, *Applied Catalysis B: Environmental*, 2009, **88**, 413.
8. H. Chang, X. Chen, J. Li, L. Ma, C. Wang, C. Liu, J. W. Schwank and J. Hao, *Environmental Science & Technology*, 2013, **47**, 5294.
9. C. Fang, D. Zhang, S. Cai, L. Zhang, L. Huang, H. Li, P. Maitarad, L. Shi, R. Gao and J. Zhang, *Nanoscale*, 2013, **5**, 9199.
10. X. Fan, F. Qiu, H. Yang, W. Tian, T. Hou and X. Zhang, *Catalysis Communications*, 2011, **12**, 1298.
11. T. Gu, R. Jin, Y. Liu, H. Liu, X. Weng and Z. Wu, *Applied Catalysis B: Environmental*, 2013, **129**, 30.
12. H. Li, X. Tang, H. Yi and L. Yu, *Journal of Rare Earths*, 2010, **28**, 64.
13. F. Liu, W. Shan, Z. Lian, L. Xie, W. Yang and H. He, *Catalysis Science & Technology*, 2013, **3**, 2699.
14. G. Marban, T. Valdes-Solis and A. B. Fuertes, *Physical Chemistry Chemical Physics*, 2004, **6**, 4534.
15. A. Patel, P. Shukla, J. Chen, T. E. Rufford, V. Rudolph and Z. Zhu, *Catalysis Today*, 2013, **212**, 38.
16. G. Qi and R. T. Yang, *Journal of Catalysis*, 2003, **217**, 434.
17. M. Richter, A. Trunschke, U. Bentrup, K. W. Brzezinka, E. Schreier, M. Schneider, M. M. Pohl and R. Fricke, *Journal of Catalysis*, 2002, **206**, 98.
18. Z. Wu, R. Jin, H. Wang and Y. Liu, *Catalysis Communications*, 2009, **10**, 935.
19. D. Fang, J. Xie, D. Mei, Y. Zhang, F. He, X. Liu and Y. Li, *RSC Advances*, 2014, **4**, 25540.
20. R. Jin, Y. Liu, Y. Wang, W. Cen, Z. Wu, H. Wang and X. Weng, *Applied Catalysis B: Environmental*, 2014, **148–149**, 582.
21. J. Zuo, Z. Chen, F. Wang, Y. Yu, L. Wang and X. Li, *Industrial & Engineering Chemistry Research*, 2014, **53**, 2647.
22. H. Jiang, J. Zhao, D. Jiang and M. Zhang, *Catal Lett*, 2014, **144**, 325.
23. X. Lu, C. Song, C.-C. Chang, Y. Teng, Z. Tong and X. Tang, *Industrial & Engineering Chemistry Research*, 2014, **53**, 11601.
24. L. Zhang, L. Shi, L. Huang, J. Zhang, R. Gao and D. Zhang, *ACS Catalysis*, 2014, **4**, 1753.
25. Y. Wan, W. Zhao, Y. Tang, L. Li, H. Wang, Y. Cui, J. Gu, Y. Li and J. Shi, *Applied Catalysis B: Environmental*, 2014, **148–149**, 114.
26. Y. Xin, P. Jiang, M. Yu, H. Gu, Q. Li and Z. Zhang, *Journal of Materials Chemistry A*, 2014, **2**, 6419.
27. B. Thirupathi and P. G. Smirniotis, *Journal of Catalysis*, 2012, **288**, 74.
28. A. Sultana, M. Sasaki and H. Hamada, *Catalysis Today*, 2012, **185**, 284.
29. D. Zhang, L. Zhang, L. Shi, C. Fang, H. Li, R. Gao, L. Huang and J. Zhang, *Nanoscale*, 2013, **5**, 1127.
30. T. S. Park, S. K. Jeong, S. H. Hong and S. C. Hong, *Industrial & Engineering Chemistry Research*, 2001, **40**, 4491.
31. S. Zhan, M. Qiu, S. Yang, D. Zhu, H. Yu and Y. Li, *Journal of Materials Chemistry A*, 2014, **2**, 20486.
32. Y. Shi, S. Chen, H. Sun, Y. Shu and X. Quan, *Catalysis Communications*, 2013, **42**, 10.
33. F. Kleitz, S. Hei Choi and R. Ryoo, *Chemical Communications*, 2003, 2136.
34. C. Zhang and J. Lin, *Physical Chemistry Chemical Physics*, 2011, **13**, 3896.
35. M. Gibert, P. Abellan, L. Martinez, E. Roman, A. Crespi, F. Sandiumenge, T. Puig and X. Obradors, *CrystEngComm*, 2011, **13**, 6719.
36. M. Kang, E. D. Park, J. M. Kim and J. E. Yie, *Catalysis Today*, 2006, **111**, 236.
37. X. Tang, J. Hao, W. Xu and J. Li, *Catalysis Communications*, 2007, **8**, 329.F. Liu, H. He, Y. Ding, C. Zhang, *Applied Catalysis B: Environmental*, 2009, **93**, 194.
38. Y. Yao, S.-l. Zhang, Q. Zhong and X.-x. Liu, *Journal of Fuel Chemistry and Technology*, 2011, **39**, 694.
39. Z. Liu, Y. Yi, S. Zhang, T. Zhu, J. Zhu and J. Wang, *Catalysis Today*, 2013, **216**, 76.
40. B. Meng, Z. Zhao, Y. Chen, X. Wang, Y. Li and J. Qiu, *Chemical Communications*, 2014, **50**, 12396.
41. F. Liu, H. He, Y. Ding and C. Zhang, *Applied Catalysis B: Environmental*, 2009, **93**, 194.
42. Z. Liu, Y. Li, T. Zhu, H. Su, J. Zhu, *Industrial & Engineering Chemistry Research*, 2014, **53**, 12964.